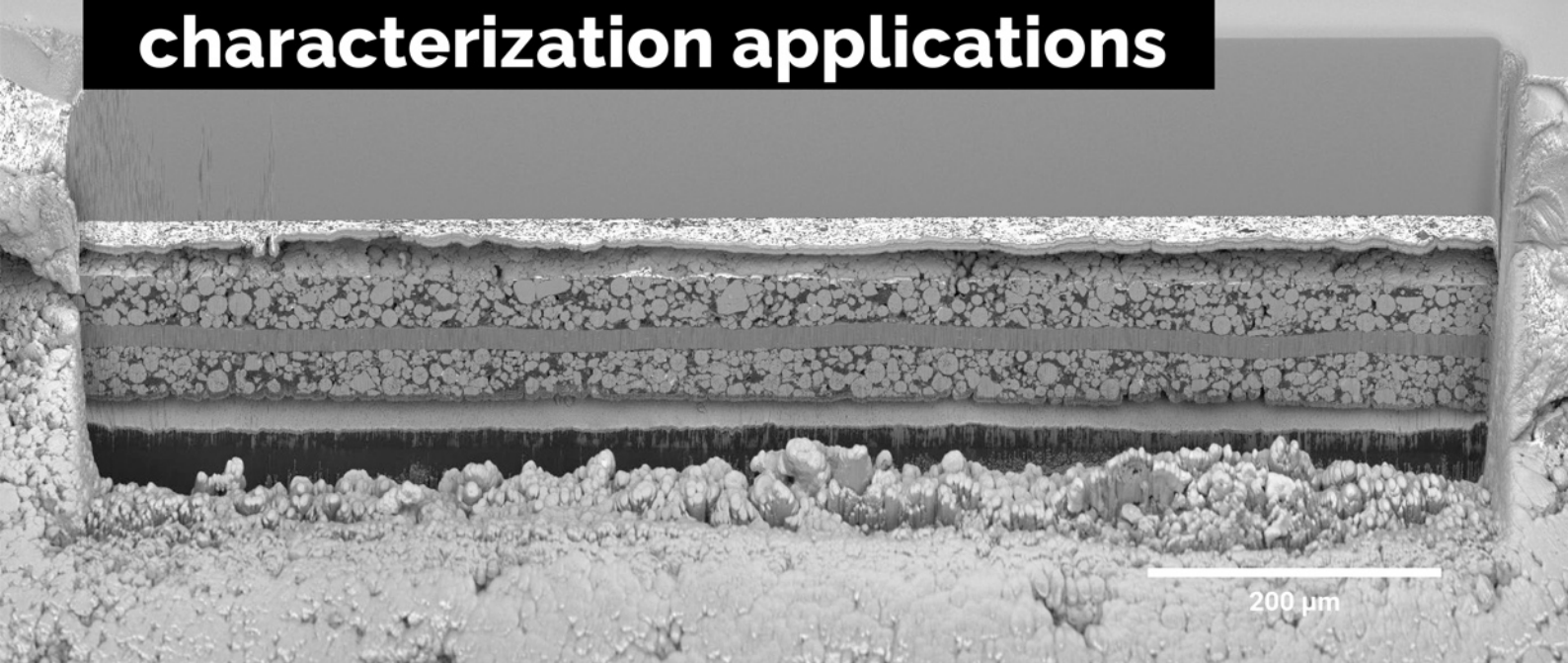


A unique combination of Plasma FIB and field-free UHR SEM for the widest range of multiscale materials characterization applications



1 mm cross-section through a Li-ion battery electrode

TESCAN AMBER X

- ✓ High throughput, large area FIB milling up to 1 mm
- ✓ Ga-free microsample preparation
- ✓ Ultra-high resolution, field-free FE-SEM imaging and analysis
- ✓ In-column SE and BSE detection
- ✓ Spot optimization for high-throughput, multi-modal FIB-SEM tomography
- ✓ Superior field of view for easy navigation
- ✓ Essence™ easy-to-use, modular graphical user interface



For more information visit

www.tescan.com

Largely Enhanced Output of the Non-Contact Mode Triboelectric Nanogenerator via a Charge Excitation Based on a High Insulation Strategy

Rui Lei, Shuyao Li, Yuxiang Shi, Peng Yang, Xinglin Tao, Hua Zhai,* Zhong Lin Wang, and Xiangyu Chen*

The non-contact triboelectric nanogenerator (TENG) based on floating plane motion can achieve a very low interface abrasion and high durability. However, the output performance of non-contact TENG is still less than $72 \mu\text{C m}^{-2}$, due to the decay of tribo-induced charges in air. Here, this work proposes two different charge excitation strategies for non-contact mode TENG by elevating the electric insulation strength to avoid air breakdown, while both the external charge excitation and the self-excitation system are developed. A double dielectric layer capacitance model is also established to analyze the change of charge density. A maximum output charge density of $260.15 \mu\text{C m}^{-2}$ is obtained using the external charge excitation with 6 kV excitation voltage. In addition, the self-excitation strategy with non-contact mode and more compact system is also demonstrated and an output charge density of $212.5 \mu\text{C m}^{-2}$ is achieved with the help of developed voltage multiple circuit, which is 2.97 times of the reported highest record for non-contact TENG. The charge-excited TENG via high electric insulation strategy realized in this work provides a promising way for boosting the output performance of TENGs.

1. Introduction

As the modern society enters the era of intelligence and information, harvesting ambient mechanical energy, such as wind,^[1] wave,^[2] vibration,^[3] human motion,^[4] etc.,^[5] provides a new idea for the power supply of distributed and moveable devices.^[6] Coupling triboelectrification and electrostatic induction, triboelectric nanogenerator (TENG) exhibits the merits of light weight, low cost, versatile selectivity of materials,^[7] making it an effective solution for ambient mechanical energy harvesting. In general, the triboelectrification effect inevitably requires the friction motions between tribo-layers, which causes interface abrasion and reduces the energy conversion efficiency.^[8] Thus, suppressing the negative effects of friction to elevate the output performance is one of the most important challenges for TENG.

Great efforts have been made in this direction, such as the use of low friction resistance materials (animal furs,^[9] elastic sheet-like polymer,^[10] etc.), the application of lubricating fluid between the contact interfaces,^[11] and the floating plane motion without interface contact.^[12] Theoretically, if we neglect the energy loss caused by friction motion, a floating non-contact TENG would have a total energy conversion efficiency $>85\%$, which greatly improve the durability of TENG. However, the residual surface charges in the non-contact mode are difficult to maintain for a long time, which greatly limits its output performance and applications.

Previous researches have proposed many methods to elevate the charge density of TENG, such as chemical modification of polymer,^[13] optimized surface contact state,^[14] utilizing the charge trapping layer,^[15] surface nano pattern,^[16] working environment control,^[17] etc. However, these methods are not enough for the non-contact mode TENGs, since the charge decay in air is a major challenge of the non-contact TENGs. To obtain a fully non-contact floating TENG without mechanical instability, the gap between the floating layer and stator should be at least hundred micrometers, which strongly suppress its energy output. As inspired by external and self-excitation system of EMG, a charge-excitation method has been proposed to overcome the limit of surface charge density of tribo-layer,^[18]

R. Lei, S. Li, Y. Shi, P. Yang, X. Tao, Z. L. Wang, X. Chen
Beijing Key Laboratory of Micro-Nano Energy and Sensor
Beijing Institute of Nanoenergy and Nanosystems
Chinese Academy of Sciences
Beijing 100083, P. R. China
E-mail: chenxiangyu@binn.cas.cn

R. Lei, H. Zhai
Anhui Province Key Lab of Aerospace Structural Parts Forming
Technology and Equipment
Hefei University of Technology
Hefei, Anhui 230009, P. R. China
E-mail: jxzhaihuajx@hfut.edu.cn

R. Lei, H. Zhai
Institute of Industry & Equipment Technology
Hefei University of Technology
Hefei, Anhui 230009, P. R. China

S. Li, Y. Shi, P. Yang, X. Tao, Z. L. Wang, X. Chen
School of Nanoscience and Technology
University of Chinese Academy of Sciences
Beijing 100049, P. R. China

Z. L. Wang
School of Material Science and Engineering
Georgia Institute of Technology
Atlanta, GA 30332-0245, USA

 The ORCID identification number(s) for the author(s) of this article can be found under <https://doi.org/10.1002/aenm.202201708>.

DOI: 10.1002/aenm.202201708

while the output charge density of TENG is even hoisted to $3530 \mu\text{C m}^{-2}$ based on charge excitation strategy and high- k material.^[19] Thus, the charge excitation method can also be a promising approach for improving the output of non-contact (floating) TENG. Very recently, utilizing a self-excited amplification method, a fully floating sliding TENG with an excitation voltage about 2 kV delivers a charge density of $71.53 \mu\text{C m}^{-2}$, reaching a milestone for non-contact TENG.^[20] However, such charge density of non-contact TENG is still relatively low due to the low withstand voltage of air.

In this work, we develop two kinds of non-contact TENG via external charge-excitation (ECEf-TENG) and self-excitation (SCEf-TENG) based on a high electric insulation strategy. By using dielectric oil with a high dielectric strength to fill the floating gap, the air-breakdown effect during the TENG operation is avoided, which greatly improve charge storage capacity of floating layer. To estimate the output charge density, a double dielectric layer capacitance model of the non-contact TENG is prepared. The ECEf-TENG is fabricated by using a low frictional resistance material and a voltage stabilization circuit (VSC), while the output charge density can be optimized by regulating many factors, such as excitation voltage, thickness and type of dielectric film, gap, etc. This system delivers an effective charge density of $260.15 \mu\text{C m}^{-2}$ with an external excitation voltage of 6 kV. Then, a developed unidirectional charge-injection voltage-multiplying circuits (VMC) is utilized to realize the fully non-contact SCEf-TENG and the charge density reaches $212.5 \mu\text{C m}^{-2}$ with 1.5 Hz low frequency, which are 2.97 times higher than the highest record of previous non-contact TENG.

This work provides a reliable method of charge excitation with high electric insulation strategy for enhancing the output of TENG and also presents core factors of high-performance non-contact TENG.

2. Results and Discussion

The basic concept of the ECEf-TENG (or SCEf-TENG) with high electric insulation is shown in Figure 1a, which consists of main TENG and charge exciter (both external charge-excitation and self-excitation). For main TENG, a floating electrode covered with dielectric film as the slider and a PCB plate printed with two electrodes as the stator, and the gap between top and bottom electrodes is filled with nonpolar dielectric oil. A conceptual pump as the high voltage charge exciter to continuously transfer the electrons from bottom electrode to the floating electrode, where the electrons are firmly bonded. From another perspective, both external and self-excitation act as the high voltage source to supply charges to the electrode of the main TENG, as shown in Figure 1b. To further explain the charge-excitation with high electric insulation strategy, the double dielectric layer capacitor model is established as shown in Figure 1c, where the capacitor consists of two electrodes (floating electrode on the slider and bottom electrode on the stator) separated by a uniform gap filled with two layers of uniform dielectrics (including dielectric film and other dielectrics, such as air or oil). The capacitance C of each model can be calculated as following equations.

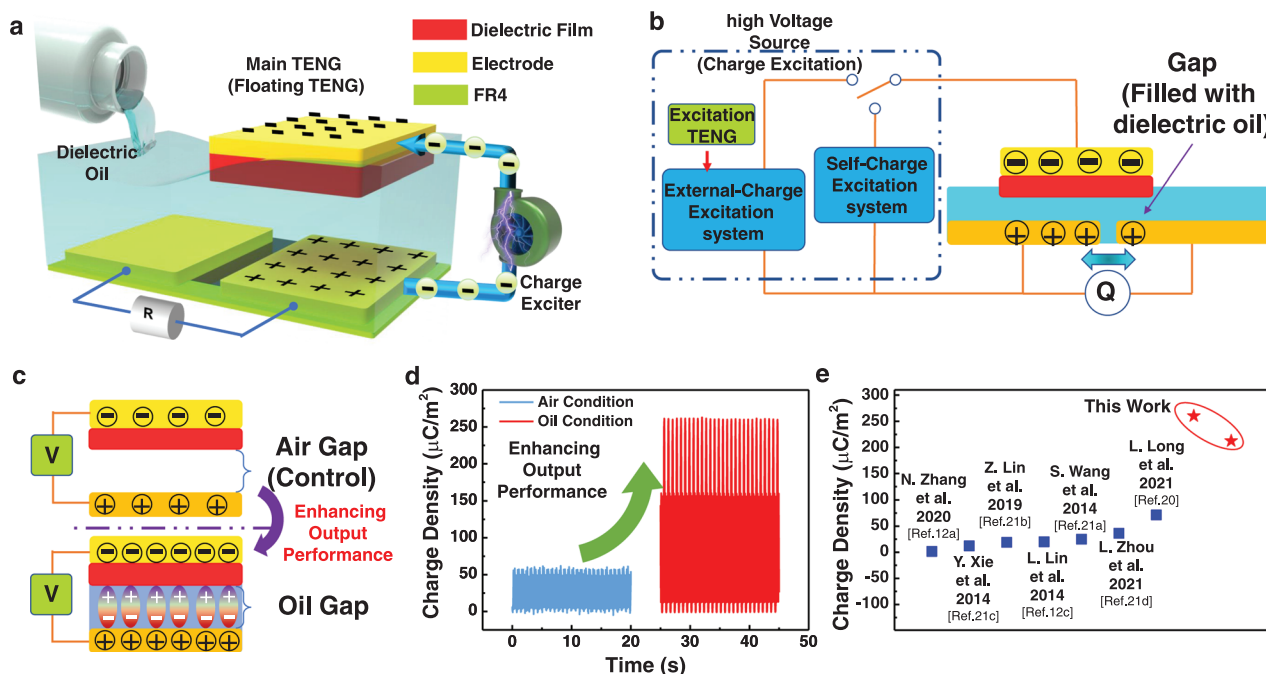


Figure 1. Design and Output performance of floating TENG via charge excitation based on high electric insulation strategy; a) Schematic illustration of floating TENG via charge excitation based on high electric insulation strategy; b) the fundamental scheme of floating TENG with external and self-charge excitation proposed in this work; c) comparison of simplified capacitance models of floating TENG between air condition and oil condition; d) comparison of output charge density of ECEf-TENG between oil condition and air condition; e) comparison of the charge density obtained in this work with other reports.

$$C_1 = \frac{\epsilon_0 S}{\frac{d_1 + d_2}{\epsilon_1}} \quad (1)$$

and

$$C_2 = \frac{\epsilon_0 S}{\frac{d_1}{\epsilon_1} + \frac{d_2}{\epsilon_2}} \quad (2)$$

Here, C_1 and C_2 are the corresponding capacitance, ϵ_0 is the vacuum permittivity, ϵ_1 and ϵ_2 are the relative permittivity of film and oil, respectively. d_1 and d_2 are the thickness of film and another dielectric (air or oil), While S is the area of each electrode. The capacitance of C_2 is larger than C_1 due to the larger relative permittivity of oil than that of air. The maximum amount of charge a capacitor can store is defined as Q_{\max} , which can be calculated as following equation.

$$Q_{\max} = CU \quad (3)$$

where U is the maximum withstand voltage of the capacitor. The voltage limit of high dielectric strength oil is much higher than that of air to obtain a higher withstand voltage of corresponding capacitor and thus, the Q_{\max} of C_2 is much greater than that of C_1 . Because the charge is firmly bounded on floating electrode, the transferred charge of TENG can be approximately considered as Q_{\max} . A maximum effective charge density of $260.15 \mu\text{C m}^{-2}$ can be realized for floating TENG with an excitation voltage of 6 kV when the gap between film and bottom electrode is filled with oil, 4.41 times than the control that the gap is filled with air, as shown in Figure 1d. Meanwhile, an effective charge density of $212.5 \mu\text{C m}^{-2}$ can be provided by a more compact SCEF-TENG system with fully non-contact mode. Such outputs of TENG systems far beyond that non-contact mode TENGs in the previous works^[12a,c,20,21] (Figure 1e). Then, the detailed design and working mechanism of both ECEF-TENG and SCEF-TENG are induced in the following part.

The structural diagram of ECEF-TENG is shown in Figure 2a. It mainly contains an excitation TENG and a main TENG, both of which are working in the sliding mode. It should be noted that the main TENG is exposed to air as the control group. The 3D structure and real photograph of the excitation TENG are illustrated in Figure 2b and Figure S1a, Supporting Information, respectively. Rabbit hair is chosen as the tribo-material owing to its superior softness and elasticity, while PTFE film is also selected for maintaining good electrification performance. To further enhance the performance of excitation TENG, rabbit hair and PTFE are all treated with fluorinert liquid (Experimental Section). After the treatment, the output of excitation TENG is improved, that the open-circuit voltage increased from 4503 to 8749 V (Figure 2c). Similarly, transferred charge increased from 0.107 to 0.197 μC , short-circuit current increased from 1.69 to 2.89 μA , and peak power increased from 1.805 to 7.22 mW at 2 G Ω (Figure S1b–d, Supporting Information). By comparing the scanning electron microscopic (SEM) images of rabbit hair and PTFE (see Figure 2c,d), the treatment does not change the surface morphology of materials. By further

analyzing the element type and content of the materials with the help of energy dispersive spectrometer (EDS), it has been found that the fluorine-carbon ratio of PTFE increases from 2.07 (before treatment) to 2.32 (after treatment) while that of rabbit hair increases from 0 to 0.098 (Figure S1e, Supporting Information). The increase of fluorine content can explain the output enhancement of excitation TENG. The VSC contains a high voltage rectifier, Zener diodes, and a buffer capacitor, which regulates the AC output voltage of excitation TENG to the DC output voltage (Figure 2a). Figure 2f shows the excitation DC voltage of ECEF-TENG regulated by Zener diodes with different stabilized voltage (the capacitance of buffer capacitor is 0.1 nF). The influence of the capacitance value of the buffer capacitor on excitation voltage is also tested. In order to have a faster excitation speed and more stable excitation voltage, four capacitors of different capacities are chosen for comparison as shown in Figure S2, Supporting Information. As the capacitance increases, the excitation time also increase, but the voltage becomes more stable. Considering the excitation time and the stability of voltage, we choose the buffer capacitor with a capacitance of 0.1 nF. The 3D structure and real photograph of main TENG are shown in Figure 2g and Figure S3, Supporting Information, respectively. The Kapton film is chosen as the dielectric film of the slider and the dried conductive ink (electrode) is directly printed on it without any Epoxy glue. The stator is a PCB board with copper electrodes and there is a uniform gap between the slider and the stator to avoid mechanical wear.

The external charge-excitation process during the periodical cycle is shown in Figure S4, Supporting Information. It should be noted that the excitation TENG is pre-charged by periodical sliding to obtain a relative stable output. Thus, in the initial state, the PTFE has few negative charges while the rabbit hair is positive charged in advance (Figure S4a, Supporting Information), and the potential between top and bottom electrodes of main TENG is zero. The rabbit hair as the slider in excitation TENG moves synchronously with the slider in main TENG. When the rabbit hair starts to slide periodically, the AC output is produced to the VSC by the potential difference between electrodes of excitation TENG, and a DC output is converted to continuously inject charges to top and bottom electrodes of the main TENG. The negatively charged electrode in slider drives the electrons in the bottom electrodes of the stator, enabling a constant AC induction output of main TENG (Figure S4b,c, Supporting Information). After a few cycles, the voltage between top and bottom electrodes reaches stability and the charge injected into the top electrode become saturated, and main TENG can provide a maximum output (Figure S4d, Supporting Information). The durability of the excitation TENG is a key issue for the continuous operation of the entire ECEF-TENG system. As shown in Figure S5, Supporting Information, after more than 35 min of continuous operation, the maximum output voltage of the excitation TENG with VSC remained stable at about 5900 V, which shows the high reliability of the excitation TENG as a voltage source.

The equivalent physical model of ECEF-TENG exposed in air is shown in Figure 2h. The voltage applied between the top and bottom electrodes is U , while the film is subjected to a voltage of U_1 and the air to a voltage of U_2 . In order to achieve maximum output, air breakdown should be avoided.

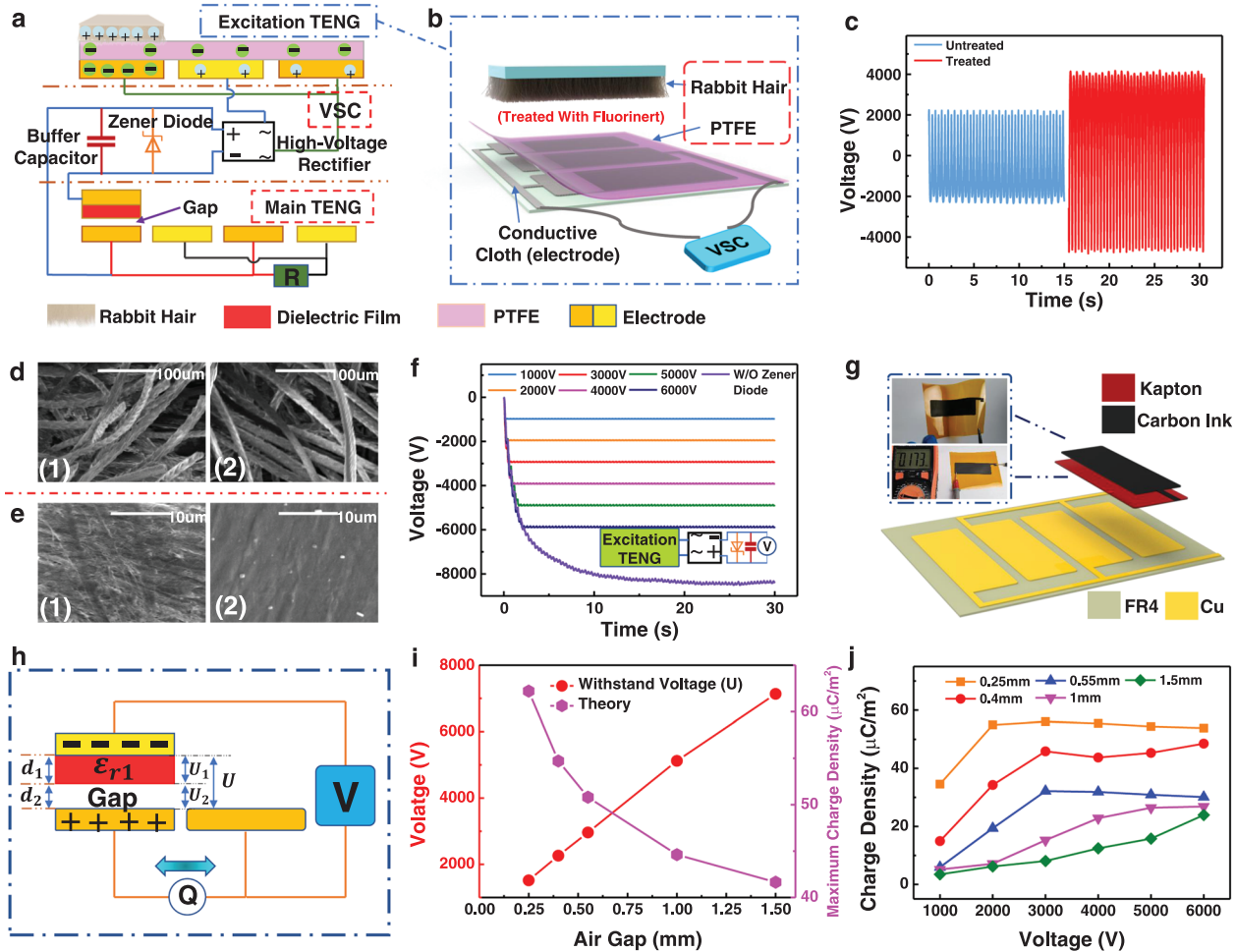


Figure 2. Design and Output performance of ECEF-TENG (control, main TENG is exposed to the air). a) Schematic illustration of ECEF-TENG; b) schematic illustration of excitation TENG. c) Rabbit hair and d) PTFE, respectively, indicating the comparison of two materials (1) before and (2) after treatment with Fluorinert; e) comparison of voltage performance of excitation TENG before and after treatment with Fluorinert; f) voltage performance of excitation TENG connected with voltage-stabilization circuit (VSC) under different stabilized voltage; g) schematic illustration of main TENG, the inset is the photograph of the slider. h) Simplified equivalent physical and electric model of ECEF-TENG (some critical parameters are shown in the schematic). i) Theoretical withstand voltages between top and bottom electrodes (without air breakdown) and maximum charge density under different air gaps; j) the plot of experimental charge density versus excitation voltage under different air gaps.

Therefore, according to Paschen's law, the voltage applied on the air follows.

$$U_2 \leq \frac{A(Pd_2)}{\ln(Pd_2) + B} \quad (4)$$

And the voltage applied between top and bottom electrodes follows.

$$U \leq \frac{AP(d_1 + \epsilon_1 d_2)}{[\ln(Pd_2) + B]\epsilon_1} \quad (5)$$

where P is the standard barometric pressure, A and B are the constants determined by atmosphere such as the composition and the pressure of the air. For ambient condition, A is $2.87 \times 10^7 \text{ V (atm} \cdot \text{m)}^{-1}$ and B is 12.6. Other parameters refer to the corresponding parameters of Equations (1) and (2).

According to the Equations (1) and (5), the maximum charge density σ_0 of the electrode can be expressed by

$$\sigma_0 = \frac{AP\epsilon_0}{\ln(Pd_2) + B} \quad (6)$$

Obviously, with the increase of air gap, the maximum charge density decreases while the applied withstand voltage between electrodes increase, as theoretical calculation plotted in Figure 2i. In order to avoid direct discharge between electrodes caused by overload of applied voltage, Kapton with $50 \mu\text{m}$ thickness (the withstand voltage value exceeds 6 kV) is used to protect the instrument.

To investigate the real output of ECEF-TENG in air condition, a programmable linear motor is utilized as the driving force for the sliders in excitation TENG and main TENG (motion frequency of 1.5 Hz). A linear guide rail is used to enable the

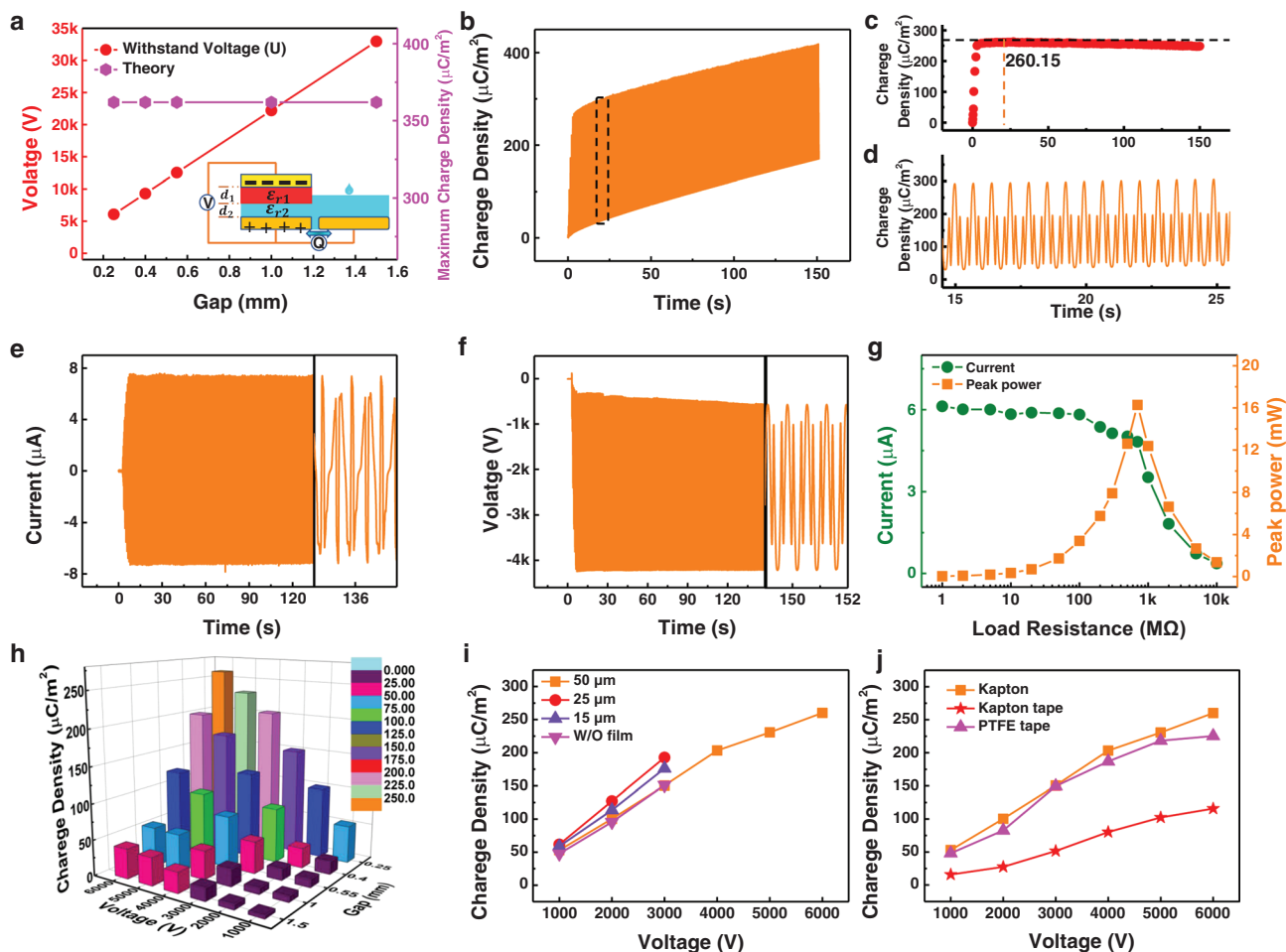


Figure 3. Output performance of ECEF-TENG (main TENG is submerged in dielectric oil). a) Theoretical threshold voltages between top and bottom electrodes (without oil breakdown), the inset is the simplified equivalent physical and electric model of ECEF-TENG submerged in dielectric oil (some critical parameters are shown in the schematic). b) The dynamic output charge accumulation process of ECEF-TENG. c) The effective charge density. d) The detailed output charge curve from the dashed area. e) Short-circuit current of ECEF-TENG, the inset is enlarged part at last few seconds; f) open-circuit voltage of ECEF-TENG, the inset is enlarged part at last few seconds; g) matching impedance and output power with 0.25 mm oil gap; h) effective charge density of ECEF-TENG with different excitation voltage and oil gaps. i) Effective charge density of ECEF-TENG with different excitation voltage and thickness of film (oil gap is fixed at 0.25 mm); j) effective charge density of ECEF-TENG with different kind of films and excitation voltage (oil gap is fixed at 0.25 mm).

gap between slider and stator in main TENG. Under certain gaps, the influence of excitation voltage changes on effective charge density is explored, as plotted in Figure 2j. Theoretically, under the gap of 0.25 mm, the maximum output of ECEF-TENG exposed in air is $59 \mu\text{C m}^{-2}$, and the maximum applied voltage between the top and bottom electrodes of main TENG is 1774 V (Figure 2i). During the experiment, air breakdown occurs when the voltage exceeds 2 kV, and the effective charge density of main TENG does not increase with the applied voltage and remains at about $55 \mu\text{C m}^{-2}$. A maximum effective charge density of $56.06 \mu\text{C m}^{-2}$ is obtained with applied voltage of 3 kV (Figure S6a, Supporting Information), and a significant shift of output occurs at initial moment due to the air breakdown. It should be noted that only a small amount of charges accumulates on the surface of the Kapton ($\approx 7 \text{ nC}$, Figure S6b, Supporting Information) and the output of main TENG is mainly derived from charge excitation process. With the

increase of air gap, the maximum withstand voltage between electrodes increase. The output charge density increases as the applied voltage increases, and the output charge density no longer increases after the applied voltage exceeds the withstand voltage between electrodes. Therefore, simply increasing the applied voltage cannot effectively enhance the output of such TENG system.

In order to realize the charge-excitation with high electric insulation strategy, we fill the air gap with dielectric oil, as shown in Video S1, Supporting Information and inset of Figure 3a. Electronics coolant liquids (FC40) is a non-polar oil with high dielectric strength, non-toxicity, low viscosity, and easy to be cleaned, which is used in this work. To test the dielectric properties of the oil, a bare Cu electrode without film protection serves as the slider of main TENG. Adjusting the gap between slider and stator of main TENG with 0.25 mm and applying the excitation voltage with 6 kV, as illustrated in

Figure S7a, Supporting Information, the breakdown voltage of oil is obtained through four experiments to take the average value (Figure S7b–e, Supporting Information). After the calculation, the average breakdown voltage of the oil is 5381.5 V with 0.25 mm gap. Generally, the slider of the main TENG has the dielectric film to prevent the direct breakdown between top and bottom electrodes. Thus, the maximum applied voltage between top and bottom electrodes is

$$U = \frac{\varepsilon_2 d_1 + \varepsilon_1 d_2}{\varepsilon_1} \cdot E_{\max} \quad (7)$$

where E_{\max} is the maximum dielectric strength of the oil. Thus, the maximum applied voltage on electrodes is estimated as 6063.1 V with a 50 μm thickness Kapton film and a 0.25 mm gap (electrical performance parameters of dielectric films and oil are listed in Table S1, Supporting Information), and the applied voltage of 6 kV is a safe voltage to prevent breakdown. The maximum charge density of main TENG can be deduced as

$$\sigma_0 = \varepsilon_0 \cdot \varepsilon_2 \cdot E_{\max} \quad (8)$$

Theoretically, a constant charge density can be achieved as long as a sufficiently excitation voltage is applied, and the maximum voltage applied on ECEF-TENG increases significantly with gap, as shown in Figure 3a. However, in the actual experiment, we limit the maximum excitation voltage to 6 kV to protect the instrument, so that the charge density expression follows.

$$\sigma_0 = \frac{C \cdot U}{S} = \frac{\varepsilon_0}{\frac{d_1}{\varepsilon_1} + \frac{d_2}{\varepsilon_2}} \cdot U \quad (9)$$

The whole deduction process of maximum charge density of the double dielectric layer capacitance is shown in Note S1, Supporting Information. We have also calculated the resistance to be overcome by the slider in oil and air, respectively (Note S1, Supporting Information). The measured charge density on main TENG with 6 kV excitation voltage and 0.25 mm gap are illustrated in Figure 3b,c. Compared with main TENG exposed in air (Figure S6a, Supporting Information), the baseline of output charge density does not shift violently, which indicates that the addition of dielectric oil can effectively avoid the air breakdown. With a moving frequency of 1.5 Hz, the effective charge density linearly increases in the initial 4 s then becomes stable and reaches a maximum value of 260.15 $\mu\text{C m}^{-2}$ at 15 s. After that, it decreases slowly, as shown in Figure 3d. The short-circuit current rise at first and then fixes at a stable current of 7.4 μA (Figure 3e), while the open-circuit voltage immediately reaches the maximum 3879 V and then decreases slowly, as illustrated in Figure 3f. Figure 3g shows the output current and power density at different resistance from 1 M Ω to 10 G Ω , and the maximum peak power reaches 16.28 mW with a matching impedance of 700 M Ω . The durability of ECEF-TENG is also examined, as shown in Figure S8a,b, Supporting Information, that the TENG system operates about 33 min and the effective charge density gradually decreases from 250.6 to 196 $\mu\text{C m}^{-2}$. The enlarged figure about the curve shape of current and

voltage signal can be seen in Figure S8c, Supporting Information, where the detailed shape of each peak signal is decided by the acceleration and deceleration of the slider as well as the edge effects between different electrodes (charge induction process).

Factors related to the effective charge density of main TENG are also explored, such as excitation voltage and gap, as shown in Figure 3h. The charge density of main TENG with different applied voltage at 0.25 mm is also illustrated in Figure S9a–e, Supporting Information. The effective charge density of main TENG increase with the increase of applied voltage at certain gap, which can be explained by Equation (3) that Q is proportional to U. While the effective charge density of main TENG is decrease with the increase of gap at certain applied voltage, which can be explained by Equations (2) and (3) that C decrease with increase of gap. The effective charge density of main TENG with lower gap is also explored, as shown in Figure S10, Supporting Information. With the gap decrease further (lower than 0.25 mm), the applied voltage on the main TENG should be decreased to prevent breakdown of oil according to Equation (7), while the maximum effective charge density would keep stable according to Equation (8) if suitable voltage is applied. It can be found that the effective charge density shows slight change with different gap distance, which is consistent with Equation (8). Meanwhile, for the non-contact mode TENG, the gap distance must be kept, in order to avoid the frictional motion. So, we selected 0.25 mm as the gap distance, which can help to maintain both charge density and stability. The thickness of film is also investigated, where the withstand voltage values of Kapton films with thickness of 15, 25, and 50 μm are larger than 1.8, 3, and 6 kV, respectively. In order to protect the measuring instrument, the excitation voltage on main TENG is limited within 3 kV for the Kapton with thickness of 15 μm , 25 μm , and without Kapton film (thickness is 0 μm). At a certain gap of 0.25 mm, the effective charge density of main TENG increase with the voltage increase from 1 to 3 kV regardless the thickness of film, which can be explain by Equation (9) that the effective charge density increase with the increase of applied voltage (U), as shown in Figure 3i, and a maximum effective charge density of 192.66 $\mu\text{C m}^{-2}$ is obtained with a 25 μm thickness of Kapton film (excitation voltage is 3 kV). Also, the effective charge density of main TENG is decrease with the increase of gap with the applied voltage of 3 kV, as shown in Figure S11, Supporting Information.

Three different types of dielectric films with 50 μm thickness are chosen for the test. Figure 3j displays the effective charge density with different kind of materials by different excitation voltage under the gap of 0.25 mm. It reveals that the effective charge density is lowest with commercial Kapton tape as the dielectric film, and the output may influence by epoxy glue. While the effective charge density of 225.32 $\mu\text{C m}^{-2}$ is obtained under the excitation voltage of 6 kV that commercial PTFE tape as the dielectric film, as shown in Figure S12a, Supporting Information. The effects of excitation voltage and gap on the effective charge density of the main TENG with commercial PTFE tape as the dielectric film are also investigated, as shown in Figure S12b, Supporting Information, which shows that the main TENG with commercial PTFE tape as the dielectric film also has good output performance. The thickness of PTFE film

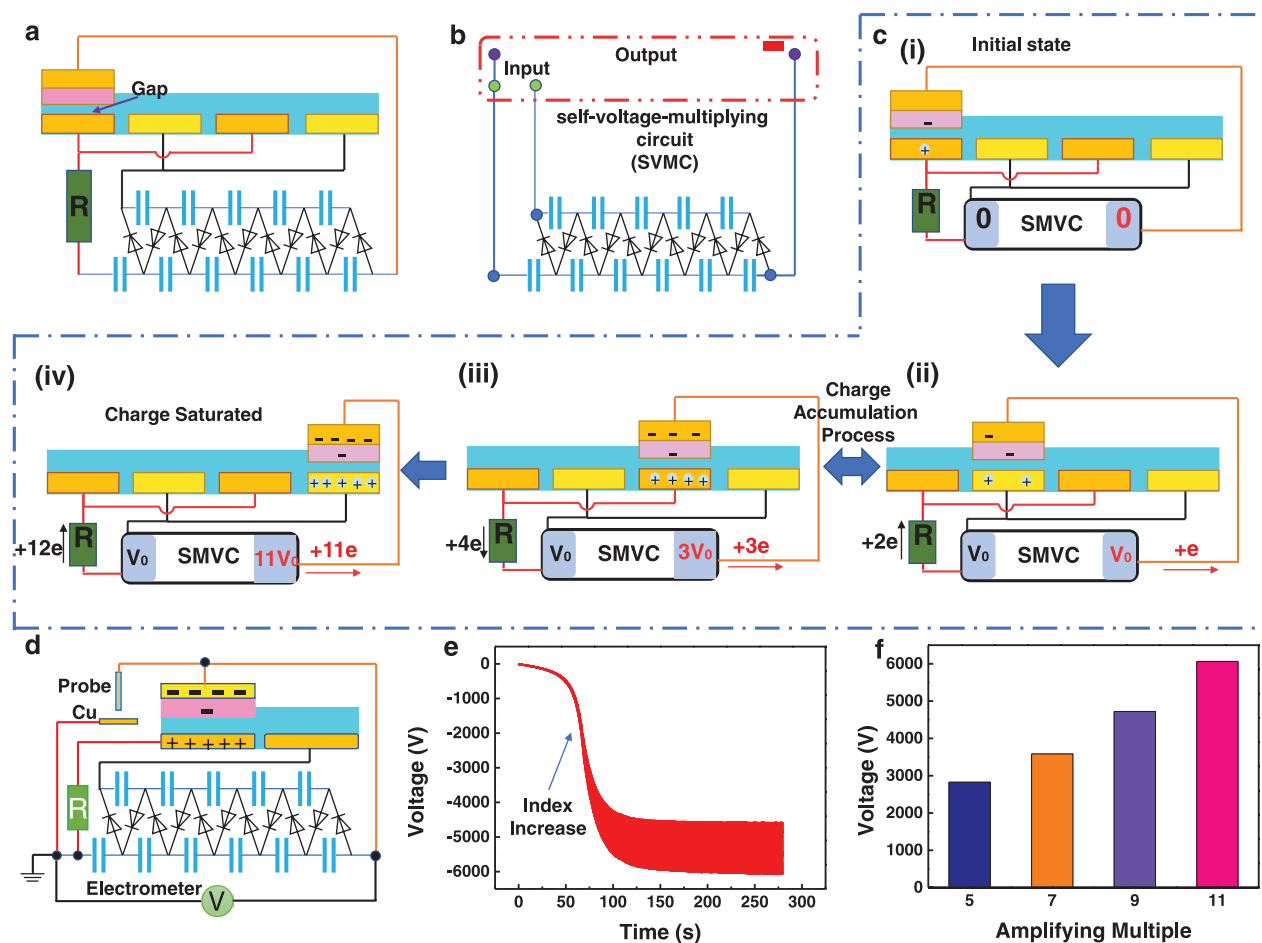


Figure 4. Structure and working principle of the SCEF-TENG. a) Schematic illustration of SCEF-TENG. b) Scheme of self-voltage-multiplying circuit (SVMC) and the input/output node. c) The charge self-excitation process of SCEF-TENG during periodically sliding cycle. d) Schematic illustration of voltage measurement between top and bottom electrodes; e) the dynamic excitation voltage between top and bottom electrodes; f) the plot of output excitation voltage between top and bottom electrodes versus voltage amplifying multiplying of SVMC.

is also investigated. At a certain gap of 0.25 mm, the effective charge density of main TENG increase with the voltage increase from 1 kV to 6 kV regardless the thickness of film, as shown in Figure S12c, Supporting Information, and the effective charge density changes slightly under certain applied voltage.

To construct a fully non-contact TENG system, an SCEF-TENG is proposed without external excitation TENG, as illustrated in Figure 4a. SCEF-TENG mainly consists of two parts, which are main TENG and the self-voltage-multiple circuit (SVMC). The detailed electric circuit scheme and the photograph of the SVMC used in this work are depicted in Figure 4b and Figure S13, Supporting Information, respectively. SVMC can be considered as a high voltage source, which consists of eleven diodes and eleven ceramic capacitors, and it theoretically forming an amplifying multiple of eleven of input voltage. It is noteworthy that the input and the output of circuit have a common node. The combination of PTFE tape (50 μm thickness) on top of slider and the dielectric oil (FC40) between slider and stator can well prevent the breakdown between top and bottom electrodes. PTFE, as an excellent electret with strong electronegativity to hold electrons, also has a very high dielectric strength (over 120 kV mm^{-1}). Therefore, PTFE not

only provides the initial charge to initiate the charge excitation process, but also protects the instrument by preventing direct breakdown between electrodes. By using rabbit hair friction in advance, PTFE is negatively charged, providing the initial charge for the self-excitation process, and the initial charge distribution of main TENG is shown in Figure S14, Supporting Information. SCEF-TENG can also be seen as an upgrade model of the ECEF-TENG system with VMC, and its evolution diagram from ECEF-TENG system with VMC is illustrated in Figure S15, Supporting Information. The charge self-excitation process during the periodical cycle is illustrated in Figure 4c. In the initial state (state i), the PTFE is pre-charged with negative charges in advance and the output voltage (excitation voltage) between output nodes of SVMC is zero. When the slider starts to move periodically, the potential difference between the electrodes of stator results in AC output (state ii). It should be noted that both input nodes of SVMC start to be charged and the output voltage increases to force the electrons continuously injecting into the top Cu electrode of slider to form a charge accumulation. The PTFE and the top Cu electrodes with negative charges work together to force the positive charges in the bottom electrodes of stator to move, enabling SCEF-TENG's

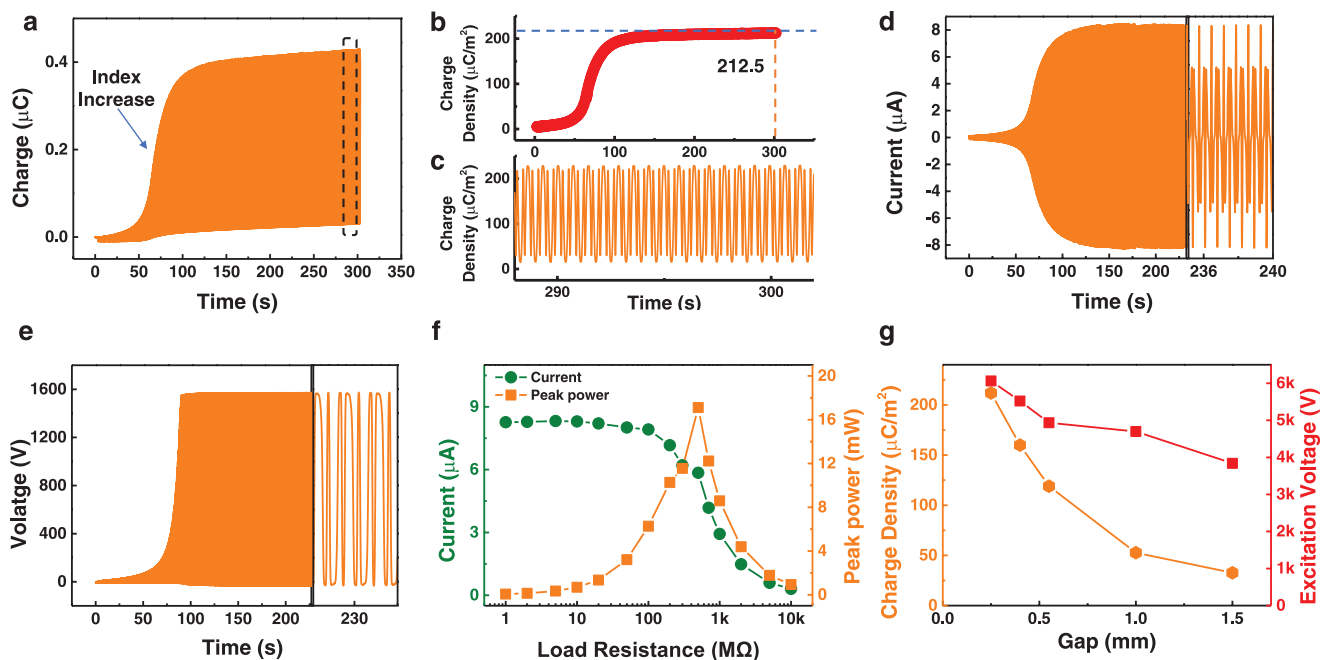


Figure 5. Output performance of SCEF-TENG. a) The dynamic output charge accumulation process of SCEF-TENG. b) The effective charge density. c) The detailed output charge density curve from the dashed area. d) Short-circuit current of SCEF-TENG, the inset is enlarged part at last few seconds; e) open-circuit voltage of SCEF-TENG (voltage between two bottom electrodes), the inset is enlarged part at last few seconds; f) matching impedance and output power with 0.25 mm oil gap; g) the plot of effective charge density of SCEF-TENG and the excitation voltage between top and bottom electrodes versus the oil gaps.

induction output to increase constantly (state iii). The voltage at both output nodes of SVMC becomes stability and the charge accumulated on the top Cu electrode tends to be saturated after several cycles, achieving a maximum output of SCEF-TENG. Thus, the charge self-excitation process is realized, as shown in state iv.

The output of the main TENG is related to the excitation voltage and gap, so the excitation voltage of the SCEF-TENG needs to be determined first. The diagrammatic illustration of excitation voltage measurement of SCEF-TENG is shown in Figure 4d, that the common node is grounded and attached to a Cu film which is 3 mm beneath the probe. The slider of SCEF-TENG is driven by the linear motor in floating mode at a frequency of 1.5 Hz. With the periodical moving of slider, the excitation voltage of SCEF-TENG exponentially increase and then stabilize to a maximum value of 6063 V with the gap of 0.25 mm, as shown in Figure 4e. The relationship between excitation voltage and the amplifying factor is investigated, as shown in Figure 4e. With the increase of the amplifying factor, the maximum excitation voltage increases and 11 is the optimized magnification in this work to generate output voltage of 6063 V. According to Equation (7), the maximum applied voltage between electrodes should be lower than 6311 V. Thus, the obtained output voltage of 6063 V is a safety value to prevent breakdown between electrodes.

The initial charge on the PTFE film is about 9.5 nC without self-excitation (0.25 mm gap), as shown in Figure S16, Supporting Information. Benefiting from the self-charge excitation process through SVMC, the transferred charge of SCEF-TENG increases exponentially from the initial 9.5 to

393 nC within 120 s at 1.5 Hz, and then gradually increase to 428.7 nC (Figure 5a). Figure 5b,c shows the effective charge density of SCEF-TENG, which needs 120 s to exponentially reach 200 $\mu\text{C m}^{-2}$ and then gradually increases to a maximum value of 212.5 $\mu\text{C m}^{-2}$. The short-circuit current exponentially reaches to a stable state within 140 s at 1.5 Hz, and then, becomes long-term stable with a stable output current of 8.37 μA (Figure 5d). The voltage between the input nodes of SVMC increases from initial 10 to 1576 V within 100 s and then becomes stable at 1600 V (Figure 5e). Figure 5f shows the current and output peak power with different resistance from 1 M Ω to 10 G Ω , and the maximum peak power reaches to 17.105 mW with the matching impedance of 500 M Ω (1.5 Hz), which is larger than 16.28 mW obtained by the ECEF-TENG. The influence of gap distance to the effective charge density and excitation voltage of SCEF-TENG are also investigated, as shown in Figure 5f. With the increase of gap, the maximum excitation voltage of SCEF-TENG gradually decrease from 6063 to 3840 V, and the effective charge density decrease from 212.5 to 32.67 $\mu\text{C m}^{-2}$ in the gaps of 0.25 to 1.5 mm, indicating that higher effective charge density can be obtained with smaller gap. Also, the thickness of PTFE film is investigated (Figure S17, Supporting Information). At a certain gap of 0.25 mm, the effective charge density of main TENG change slightly. An effective charge density of 197.33 $\mu\text{C m}^{-2}$ with a maximum excitation voltage of 5811.3 V is obtained with a thickness of 80 μm , while an effective charge density of 204.95 $\mu\text{C m}^{-2}$ with a maximum excitation voltage of 5910.5 V is obtained with a thickness of 100 μm . In addition, the stability test of the SCEF-TENG is illustrated in Figure S18b, Supporting Information, from which we can clearly see the

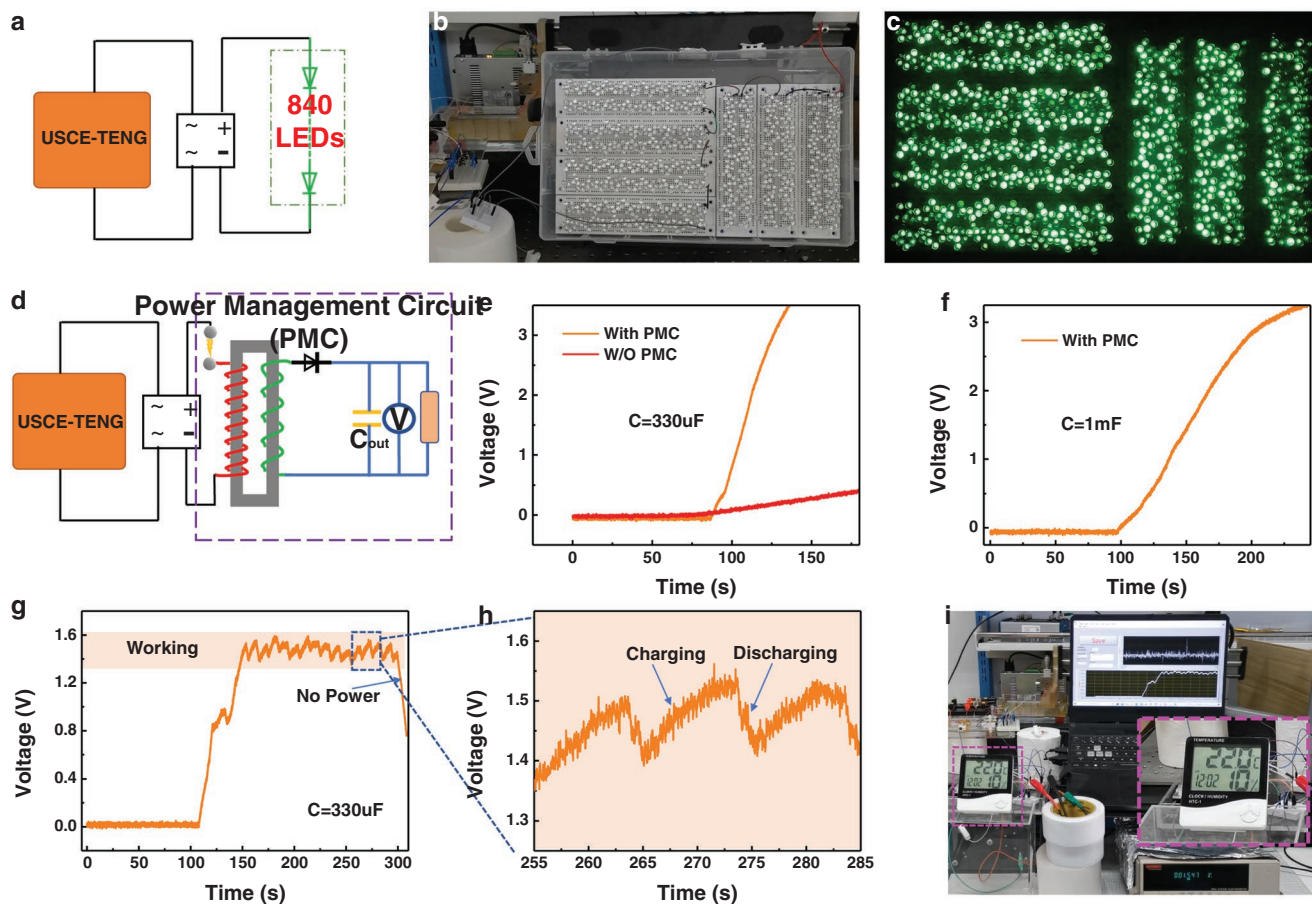


Figure 6. Application of SCEF-TENG to drive devices. a) Circuit diagram and b) real photographs of the SCEF-TENG to drive 840 LEDs, and c) 840 LEDs are lighted up in dark environment; d) circuit diagram of SCEF-TENG with an power management circuit (PMC) for powering electronic equipment. e) Charging curves of 330 μF capacitor with SCEF-TENG by using or W/O using PMC; f) Charging curves of 1 mF capacitor with SCEF-TENG by using PMC; g) voltage–time curve of temperature hygrometers with the PMC. h) The detailed voltage curve of the selected area in (g). i) The real photograph of the temperature hygrometers driven by SCEF-TENG.

maximum charge density of the SCEF-TENG is reduced from 210.43 to 195.49 $\mu\text{C m}^{-2}$ (the charge retention is 92.9%) after 35 min.

To demonstrate the output performance of SCEF-TENG in practical applications, the output is rectified to light 840 green LEDs in series at 1.5 Hz and its circuit diagram is shown in **Figure 6a**. As shown in Video S2, Supporting Information, the small amount of initial charges on the PTFE film are not enough to drive the LEDs in the initial state. With the continuous accumulation of charges on the electrode of slider, the short-circuit current of the SCEF-TENG increases exponentially and reaches a stable state, at which the LEDs are lighted up effectively with high brightness in bright and dark environments, as shown in **Figure 6b,c**. A step-down circuit, which consists of a spark switch with spacing of 0.5 mm (the working voltage is ≈ 1.5 kV), a customized transformer with transformer ratio of 15:1, and a diode, is connected into the SCEF-TENG as the power management circuit (PMC) to manage the output for low frequency energy harvesting, as shown in **Figure 6d** and **Figure S19**, Supporting Information. With the help of PMC, a capacitor of 330 μF is charged to 3.5 V within 140 s at 1.5 Hz, much faster than that charging process without

PMC (**Figure 6e**). It noteworthy that the PMC do not work for the first 90 s, due to the charge accumulation process of the SCEF-TENG to achieve the open-circuit voltage of 1.6 kV. When the voltage of the SCEF-TENG increasing exponentially and reaching the working voltage of the PMC (≈ 1.5 kV), the PMC start to work. A capacitor of 1 mF also can be charge to 3.2 V within 300 s at 1.5 Hz, as illustrated in **Figure 6f**. A commercial thermo-hygrometer is effectively driven for the sustainable working mode when the PMC is working, as shown in Video S3, Supporting Information and **Figure 6g,h** is the enlarged detail voltage curve of plotted area. **Figure 6i** is the real photograph of powering the commercial thermo-hygrometer. The applications above prove that the SCEF-TENG can be the power supply for practical applications continuously.

3. Conclusion

In summary, two kinds of non-contact TENG via external charge-excitation (ECEF-TENG) and self-excitation (SCEF-TENG) based on a high electric insulation strategy are developed. With the help of high dielectric strength oil, the

air-breakdown effect is effectively avoided during the TENG operation, leading to a higher output performance of TENG system. In addition, a theoretical model with double dielectric layer capacitor is established to optimize the output performance of non-contact TENG. A maximum effective charge density of $260.15 \mu\text{C m}^{-2}$ is obtained for ECEF-TENG at 0.25 mm gap with an external excitation voltage of 6 kV. Then, with the help of developed voltage multiple circuit, a fully non-contact SCEF-TENG with more compact system is designed to obtain a $212.5 \mu\text{C m}^{-2}$ of effective charge density with 1.5 Hz low frequency, which are 2.97 times of the highest record of non-contact TENG in previous works. Furthermore, SCEF-TENG is applied to drive 840 LEDs directly, and continuously power the commercial thermo-hygrometer with power management circuit in low frequency (1.5 Hz). This work provides a new solution for enhancing the output performance of non-contact TENG, which could further broaden the application of floating TENGs to a new horizon. The proposed TENG can be suitable for the vibration monitoring for the pipeline of chemical factories, the operation detection for engines and wheels of high-speed trains, and so on. More importantly, this kind non-contact mode TENG can be quite suitable for collecting the ocean wave energy, which can be further applied for powering offshore buoy, drilling platform and many related scenarios.

4. Experimental Section

Fabrication of Excitation TENG: In order to accurately measure the output performance of ECEF-TENG by linear motor, the sliders of excitation TENG and that of the main TENG were assembled on a substrate made by 3D printing to ensure the synchronous movement of the sliders. The slider of excitation TENG: rabbit hair was cut into the shape of rectangle with a dimension of $75 \text{ mm} \times 35 \text{ mm} \times 5 \text{ mm}$, and then be adhered to an acrylic substrate with same area by VHB tape. The stator of excitation TENG: Conductive cloth was pasted on an acrylic substrate with a dimension of $120 \text{ mm} \times 100 \text{ mm} \times 5 \text{ mm}$, and then be cut into three electrodes ($75 \text{ mm} \times 35 \text{ mm}$) with a 5 mm distance between them. The excess conductive cloth was removed and the electrodes were connected with wires. PTFE as the tribo-layer was covered on the electrodes. VSC: The high-voltage rectifier is composed of four high-voltage diodes, and the withstand voltage value of each diode is 10 kV. The nominal stabilized voltage of each Zener diode is 200 V. We connected 30 Zener diodes in series to realize the stabilized voltage of 6 kV. It should be noted that the actual stabilized voltage obtained by connecting multiple Zener diodes in series is lower than the theoretical stabilized value due to the individual differences. For example, the theoretical stabilized voltage of 6 kV can only get the actual stabilized voltage with 5.9 kV. A high-voltage porcelain chip capacitor with a 10 kV withstand voltage was chosen as the buffer capacitor. The Fluorinert was applied to the surface of PTFE and spread it evenly with the rabbit hair of slider, then air-dry the PTFE and the fluoride solution on the rabbit hair and use a comb to smooth out the rabbit hair.

Fabrication of Main TENG: The stator of main TENG was a rectangle PCB board ($120 \text{ mm} \times 100 \text{ mm} \times 1.5 \text{ mm}$) with two pairs of printing Cu electrodes ($75 \text{ mm} \times 35 \text{ mm} \times 0.15 \text{ mm}$) and the distance between each electrode was 3 mm. The stator was placed in an acrylic box ($180 \text{ mm} \times 110 \text{ mm} \times 30 \text{ mm}$) and soaked with dielectric oil (FC40). The slider of main TENG in ECEF-TENG: The rectangular PET film with thickness of $150 \mu\text{m}$ was used as a mask to cut a rectangular hole with a size of $75 \text{ mm} \times 35 \text{ mm}$ by a laser cutting machine. The mask was laid on the Kapton film with a thickness of $50 \mu\text{m}$, then evenly applied the conductive ink on the mask, and leveled the ink with a scraper. After that, the mask was removed to obtain a conductive ink electrode with a size

of $75 \text{ mm} \times 35 \text{ mm} \times 0.15 \text{ mm}$ plated on Kapton. The Kapton with electrode was put in an oven for half an hour at a temperature of $75 \text{ }^\circ\text{C}$ and dried the conductive ink to make the electrode firmly plate on Kapton. Then, the Kapton with electrode was adhered on an acrylic substrate with dimension of $75 \text{ mm} \times 35 \text{ mm} \times 5 \text{ mm}$. The slider of main TENG in SCEF-TENG: A rectangle PCB board ($85 \text{ mm} \times 35 \text{ mm} \times 1.5 \text{ mm}$) with printing Cu electrode ($75 \text{ mm} \times 35 \text{ mm} \times 0.15 \text{ mm}$) was covered with PTFE film ($50 \mu\text{m}$ of film, the epoxy glue is $15 \mu\text{m}$), and then be adhered to an acrylic plate ($85 \text{ mm} \times 35 \text{ mm} \times 5 \text{ mm}$). A micro displacement table was assembled to the slider to adjust the gap between stator and slider.

Electrical Measurement and Characterization: The sliders of TENG were driven by a linear motor (Lin-Mot S01-72/500). The transferred charge and the short-circuit current of the TENG were measured by an electrometer (Keithley 6514). It should be noted that a high voltage resistor with $1 \text{ M}\Omega$ resistance was connected into the loop circuit of TENG to protect the Keithley 6514 when measuring the transferred charge. The open-circuit voltage of TENG, voltage on VSC and voltage on SVMC were measured by a high-speed electrostatic voltmeter (Trek 341B). For the SVMC, the maximum working voltage of diode was 1 kV and the capacitance of all capacitors was 2.2 nF . The surface microscopic appearance and X-ray energy dispersive spectrum of materials were measured by scanning electron microscopy (SEM, Hitachi 8020).

Supporting Information

Supporting Information is available from the Wiley Online Library or from the author.

Acknowledgements

This work was supported by National Natural Science Foundation of China (Grant No. 62174014), Beijing Natural Science Foundation (4192069), the Beijing Municipal Science & Technology Commission (Z171100000317001), Young Top-Notch Talents Program of Beijing Excellent Talents Funding (2017000021223ZK03), Beijing Nova program (Z201100006820063), and Youth Innovation Promotion Association CAS (2021165).

Conflict of Interest

The authors declare no conflict of interest.

Data Availability Statement

The data that support the findings of this study are available from the corresponding author upon reasonable request.

Keywords

charge density, non-contact mode, self-excitation, triboelectric nanogenerators

Received: May 19, 2022

Revised: August 5, 2022

Published online:

[1] P. Veers, K. Dykes, E. Lantz, S. Barth, L. B. Carlo, O. Carlson, A. Clifton, J. Green, P. Green, H. Holtinen, D. Laird, V. Lehtomäki,

- K. L. Julie, J. Manwell, M. Marquis, C. Meneveau, P. Moriarty, X. Munduate, M. Muskulus, J. Naughton, L. Pao, J. Paquette, J. Peinke, A. Robertson, J. S. Rodrigo, M. S. Anna, J. C. Smith, A. Tuohy, R. Wiser, *Science* **2019**, 366, eaau2027.
- [2] J. Scruggs, P. Jacob, *Science* **2009**, 323, 1176.
- [3] M. Han, H. Wang, Y. Yang, C. Liang, W. Bai, Z. Yan, H. Li, Y. Xue, X. Wang, B. Akar, H. Zhao, H. Luan, J. Lim, I. Kandela, G. A. Ameer, Y. Zhang, Y. Huang, J. A. Rogers, *Nat. Electron.* **2019**, 2, 26.
- [4] a) Y. Song, J. Min, Y. Yu, H. Wang, Y. Yang, H. Zhang, W. Gao, *Sci. Adv.* **2020**, 6, eaay9842; b) T. Lee, I. Kim, D. Kim, *Adv. Electron. Mater.* **2021**, 7, 2100785.
- [5] V. Iyer, H. Gaensbauer, T. L. Daniel, S. Gollakota, *Nature* **2022**, 603, 427.
- [6] Z. L. Wang, *Nano Energy* **2019**, 58, 669.
- [7] a) Z. L. Wang, J. Chen, L. Lin, *Energy Environ. Sci.* **2015**, 8, 2250; b) A. Yu, Y. Zhu, W. Wang, J. Zhai, *Adv. Funct. Mater.* **2019**, 29, 1900098; c) M. L. R. Liman, M. T. Islam, M. M. Hossain, *Adv. Electron. Mater.* **2022**, 8, 2100578.
- [8] a) L. Lin, Y. Xie, S. Niu, S. Wang, P.-K. Yang, Z. L. Wang, *ACS Nano* **2015**, 9, 922; b) H. Guo, J. Chen, M.-H. Yeh, X. Fan, Z. Wen, Z. Li, C. Hu, Z. L. Wang, *ACS Nano* **2015**, 9, 5577.
- [9] a) P. Chen, J. An, R. Cheng, S. Shu, A. Berbillé, T. Jiang, Z. L. Wang, *Energy Environ. Sci.* **2021**, 14, 4523; b) J. Han, Y. Feng, P. Chen, X. Liang, H. Pang, T. Jiang, Z. L. Wang, *Adv. Funct. Mater.* **2022**, 32, 2108580.
- [10] a) J. Chen, X. Wei, B. Wang, R. Li, Y. Sun, Y. Peng, Z. Wu, P. Wang, Z. L. Wang, *Adv. Energy Mater.* **2021**, 11, 2102106; b) P. Wang, L. Pan, J. Wang, M. Xu, G. Dai, H. Zou, K. Dong, Z. L. Wang, *ACS Nano* **2018**, 12, 9433.
- [11] a) L. Zhou, D. Liu, Z. Zhao, S. Li, Y. Liu, L. Liu, Y. Gao, Z. L. Wang, J. Wang, *Adv. Energy Mater.* **2020**, 10, 2002920; b) J. Wu, Y. Xi, Y. Shi, *Nano Energy* **2020**, 72, 104659.
- [12] a) N. Zhang, C. Qin, T. Feng, J. Li, Z. Yang, X. Sun, E. Liang, Y. Mao, X. Wang, *Nano Res.* **2020**, 13, 1903; b) W.-Z. Song, X.-X. Wang, H.-J. Qiu, Q. Liu, J. Zhang, Z. Fan, M. Yu, S. Ramakrishna, H. Hu, Y.-Z. Long, *Nano Energy* **2019**, 63, 103878; c) L. Lin, S. Wang, S. Niu, C. Liu, Y. Xie, Z. L. Wang, *ACS Appl. Mater. Interfaces* **2014**, 6, 3031.
- [13] a) Y. Feng, Y. Zheng, S. Ma, D. Wang, F. Zhou, W. Liu, *Nano Energy* **2016**, 19, 48; b) P.-Y. Feng, Z. Xia, B. Sun, X. Jing, H. Li, X. Tao, H.-Y. Mi, Y. Liu, *ACS Appl. Mater. Interfaces* **2021**, 13, 16916; c) R. u. S. Ahmad, A. Haleem, Z. Haider, U. P. Claver, A. Fareed, I. Khan, M. K. Mbogba, K. Memon, W. Ali, W. He, P. Hu, G. Zhao, *Adv. Electron. Mater.* **2020**, 6, 2000034.
- [14] a) W. Yang, X. Wang, H. Li, J. Wu, Y. Hu, Z. Li, H. Liu, *Nano Energy* **2019**, 57, 41; b) Y. Liu, W. Liu, Z. Wang, W. He, Q. Tang, Y. Xi, X. Wang, H. Guo, C. Hu, *Nat. Commun.* **2020**, 11, 1.
- [15] a) K. Shrestha, S. Sharma, G. B. Pradhan, T. Bhatta, P. Maharjan, S. M. S. Rana, S. Lee, S. Seonu, Y. Shin, J. Y. Park, *Adv. Funct. Mater.* **2022**, 32, 2113005; b) M. T. Rahman, S. M. S. Rana, M. Salauddin, M. A. Zahed, S. Lee, E.-S. Yoon, J. Y. Park, *Nano Energy* **2022**, 100, 107454; c) S. M. S. Rana, M. A. Zahed, M. T. Rahman, M. Salauddin, S. H. Lee, C. Park, P. Maharjan, T. Bhatta, K. Shrestha, J. Y. Park, *Adv. Funct. Mater.* **2021**, 31, 2105110.
- [16] a) M.-L. Seol, J.-H. Woo, D.-I. Lee, H. Im, J. Hur, Y.-K. Choi, *Small* **2014**, 10, 3887; b) R. Mohammadpour, *Adv. Eng. Mater.* **2018**, 20, 1700767.
- [17] a) J. Wang, C. Wu, Y. Dai, Z. Zhao, A. Wang, T. Zhang, Z. L. Wang, *Nat. Commun.* **2017**, 8, 1; b) J. Fu, G. Xu, C. Li, X. Xia, D. Guan, J. Li, Z. Huang, Y. Zi, *Adv. Sci.* **2020**, 7, 2001757; c) M.-L. Seol, J.-W. Han, D.-I. Moon, M. Meyyappan, *Nano Energy* **2017**, 39, 238.
- [18] a) W. Liu, Z. Wang, G. Wang, G. Liu, J. Chen, X. Pu, Y. Xi, X. Wang, H. Guo, C. Hu, *Nat. Commun.* **2019**, 10, 1; b) L. Xu, T. Z. Bu, X. D. Yang, C. Zhang, Z. L. Wang, *Nano Energy* **2018**, 49, 625; c) L. Cheng, Q. Xu, Y. Zheng, X. Jia, Y. Qin, *Nat. Commun.* **2018**, 9, 1.
- [19] S. Fu, W. He, Q. Tang, Z. Wang, W. Liu, Q. Li, C. Shan, L. Long, C. Hu, H. Liu, *Adv. Mater.* **2022**, 34, 2105882.
- [20] L. Long, W. Liu, Z. Wang, W. He, G. Li, Q. Tang, H. Guo, X. Pu, Y. Liu, C. Hu, *Nat. Commun.* **2021**, 12, 1.
- [21] a) S. Wang, Y. Xie, S. Niu, L. Lin, Z. L. Wang, *Adv. Mater.* **2014**, 26, 2818; b) Z. Lin, B. Zhang, H. Guo, Z. Wu, H. Zou, J. Yang, Z. L. Wang, *Nano Energy* **2019**, 64, 103908; c) Y. Xie, S. Wang, S. Niu, L. Lin, Q. Jing, J. Yang, Z. Wu, Z. L. Wang, *Adv. Mater.* **2014**, 26, 6599; d) L. Zhou, Y. Gao, D. Liu, L. Liu, Z. Zhao, S. Li, W. Yuan, S. Cui, Z. L. Wang, J. Wang, *Adv. Energy Mater.* **2021**, 2101958.